

Finite element analysis of cyclically-loaded steel pipes during deep water reeling installation

Giannoula Chatzopoulou^a, Spyros A. Karamanos^{a,*}, George E. Varelis^{b,1}

^a Department of Mechanical Engineering, University of Thessaly, Volos, Greece

^b PDL Solutions (Europe) Ltd, Hexham, United Kingdom

ARTICLE INFO

Article history:

Received 27 December 2015

Received in revised form

5 May 2016

Accepted 17 July 2016

Keywords:

Offshore pipeline

Reeling

Cyclic plasticity

Structural Stability

Seamless pipe

ABSTRACT

Thick-walled steel pipes during their installation in deep water are subjected to combined loading of external pressure and bending, which may trigger structural instability due to excessive pipe ovalization. In the case of reeling installation method, prior to deep-water installation the pipe is subjected to cold forming associated with strong cyclic bending on the reel, resulting in the development of initial ovalization and residual stresses, which may affect the pipe structural performance. Using advanced material models and finite element tools, the present study examines the effect of cyclic loading due to reeling on the mechanical behavior of thick-walled seamless steel pipes. In particular, it examines the effects of reeling on cross-sectional ovalization and the corresponding material anisotropy and, most importantly, on pipe resistance against external pressure and pressurized bending. The results show that cyclic bending due to the reeling process induces significant anisotropy and ovalization on the pipe. It is also shown that the mechanical resistance of reeled pipes is lower than the resistance of non-reeled pipes, mainly because of the resulting cross-sectional ovalization at the end of reeling process.

© Published by Elsevier Ltd.

1. Introduction

Pipe reeling is an efficient installation method suitable for steel pipes of diameter up to 16 in. Kyriakides and Corona (2007). The reeling method, shown in Fig. 1, allows for controlled onshore girth welding of a long pipe segment, which is spooled onto a large diameter reel. The reeled pipe is loaded on a reeling vessel, in order to be transported, deployed and installed offshore. Once the offshore installation location is reached, the pipe is installed in deep water by unspooling as the vessel moves, with the configuration shown in Fig. 1 (Kyriakides and Corona, 2007).

The repeated “excursions” of the pipe material into the plastic range during the reeling process ovalize the pipe cross section, causing permanent (residual) stresses, influencing the pipe material mechanical properties and affecting the structural performance of the reeled pipe. In particular, the pipe experiences large strains when it is spooled onto the reel, often in the range of 2%, which requires that the pipe is mechanically straightened out before its installation. The five consecutive steps of reeling process are shown in Fig. 1 and are discussed in a later section.

The effects of reeling-induced imperfections and their importance in terms of the structural strength and stability of the steel pipe have been studied by Brown et al. (2004), who examined the definition of the minimum reelable pipe thickness. Manouchehri et al. (2008) reported the effect of the reeling installation method on the strength limit states. The interaction between residual stresses and fracture behavior of the pipe has been examined by Zhang et al. (2004), while Sriskandarajah and Rao (2015) focused on the prediction of residual ovality due to reeling process.

Upon unreeling and straightening, the pipe is installed in deep-water, where buckling under external pressure constitutes a fundamental limit state for the design of offshore pipelines, and the corresponding failure is commonly mentioned as “collapse” (Kyriakides and Corona, 2007), associated with a flattened “dog-bone” shape of the pipe cross-section. Moreover, at the sagbend region (Fig. 1) the pipe undergoes significant bending in the presence of high external pressure (Corona and Kyriakides, 1988; Karamanos and Tassoulas, 1991), which accentuates ovalization of the pipe cross section resulting in pipeline collapse. Experimental and numerical studies on the collapse pressure of reeled offshore pipes have been reported in (Pasqualino et al., 2004; Pasqualino and Neves, 2010), aimed at examining the effect of reeling-induced ovalization on pipeline performance in terms of external pressure resistance.

The effect of reeling-induced plastic deformations on pipe

* Corresponding author.

E-mail addresses: chatzopoulougiannoula@gmail.com (G. Chatzopoulou), skara@mie.uth.gr (S.A. Karamanos).

¹ Formerly at Dept. of Mechanical Engineering, University of Thessaly, Volos, Greece.

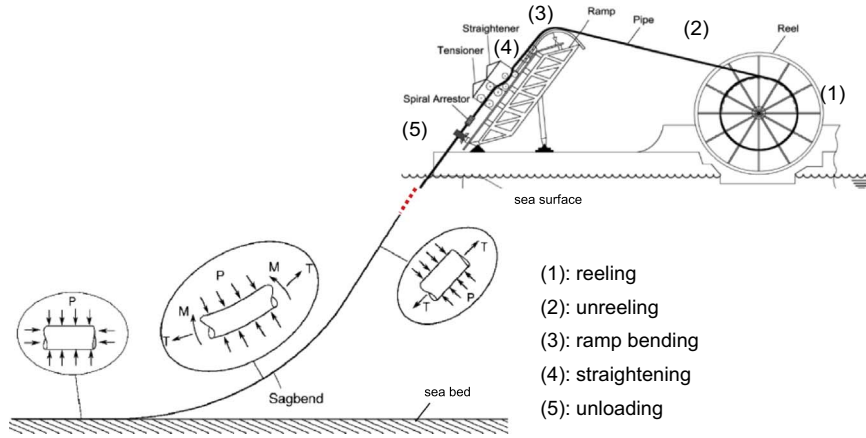


Fig. 1. Typical reeling pipeline installation vessel (Kyriakides and Corona, 2007).

material properties has been investigated during the last decade. Martinez and Brown (2005) examined the evolution of pipe properties during the reeling process. Bawood and Kenny (Dawood and Kenny, 2013) reported simulation results of the pipe mechanical response during reel-lay installation. In the work of Meiwes et al. (2014a, 2014b), small and large scale reeling tests are reported, simulating the reeling process and examining its influence on the mechanical properties of the pipe material. The effect of low temperatures on the reeling installation has been examined by Heier et al. (2013), whereas, the effect of geometric and material discontinuities at adjacent pipe segments on pipe mechanical behavior during reeling has been examined by Kyriakides and Liu (2014).

In the present study, motivated by the reeling process, the effect of cyclic bending on the mechanical response of thick-walled seamless pipes under combined loading conditions is examined using an efficient finite element model. The pipes under consideration are 12-inch-diameter seamless pipes with thickness ranging from 0.6 in to 0.937 in, which are typical for deep water applications. To describe steel material behavior, a cyclic-plasticity material model is employed, introduced by the authors elsewhere (Chatzopoulou et al., 2016). The model is based on von Mises plasticity and the nonlinear kinematic hardening rule, appropriately enhanced to account for the yield plateau at initial yielding and the Bauschinger effect. The constitutive model is numerically implemented and inserted within the finite element model using a material user-subroutine. The finite element analysis is based on a generalized two-dimensional model, capable of describing accurately cross-sectional ovalization, which is the major failure mode in the case of pressure and pressurized bending of relatively thick-walled pipes in a rigorous and accurate manner. A parametric analysis is also conducted with emphasis on the effects of cyclic bending due to reeling on the ultimate capacity of the pipe under external pressure and bending.

2. Numerical modeling

2.1. Finite element modeling description

A quasi two-dimensional model is developed in the general-purpose finite element program ABAQUS/Standard, which describes the cross-sectional deformation of the pipe under generalized plane-strain conditions. This allows for the simulation of pipe cyclic bending due to reeling, and the external pressure and bending application in a continuous multi-step analysis procedure. The present study focuses on relatively thick-walled steel pipes,

which are expected to fail primarily due to cross sectional ovalization (collapse), so that localized buckling phenomena (pipe wall wrinkling) are not dominant and, therefore, this two-dimensional analysis approach is adequate for the purpose of the present analysis. In the analysis a “half pipe” model is considered, accounting for symmetry with respect to the yz-plane (Fig. 2) and bending is applied about the x-axis of the pipe cross-section. An in-house user-defined material subroutine (UMAT) is used for the description of the material behavior under severe plastic loading conditions, presented in the subsequent Section 2.2. The pipe is discretized using four-noded, reduced-integration generalized plane-strain continuum finite elements, denoted as CPE4R in ABAQUS/Standard. In Fig. 2 the finite element model, the applied boundary conditions and the finite element mesh are depicted; five elements are employed through pipe thickness. Cyclic bending loading is applied first in five consecutive steps, followed by the application of external pressure and bending in subsequent analysis steps.

2.2. Constitutive modeling

An accurate simulation of material behavior under reverse (cyclic) loading conditions is of major importance for the accurate modeling of the reeling process and the reliable prediction of pipe capacity. During cyclic bending due to reeling/unreeling, the material behavior is characterized by two main features: (a) the yield plateau of the steel stress-strain curve upon initial yielding, (b) the Bauschinger effect under reverse plastic loading. Both features need to be taken into account in the constitutive model.

In the present study, the elastic-plastic behavior of the steel pipe material is described through a Von Mises plasticity model with nonlinear kinematic hardening initially introduced as reported in (Chatzopoulou et al., 2016). The Von Mises yield surface is given by the following equation:

$$F = \frac{1}{2}(\mathbf{s} - \mathbf{a}) \cdot (\mathbf{s} - \mathbf{a}) - \frac{k^2}{3} = 0 \quad (1)$$

where \mathbf{s} is the deviatoric stress tensor, \mathbf{a} is the “back stress” tensor and k is the size of the yield surface. The value of k is a function of the equivalent plastic strain ε_q representing material hardening, so that $k = k(\varepsilon_q)$. The evolution of the back stress tensor is given by the following expression:

$$\dot{\mathbf{a}} = C\dot{\varepsilon}^p - \gamma\mathbf{a}\dot{\varepsilon}_q \quad (2)$$

where C, γ are nonlinear kinematic hardening parameters, calibrated from appropriate material testing results.

To represent the aforementioned main two features of steel

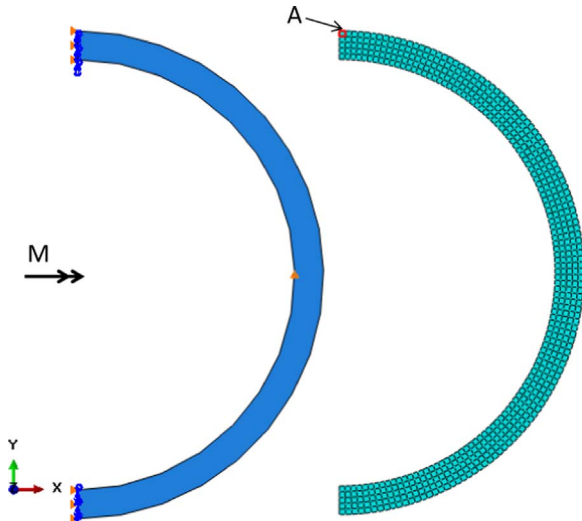


Fig. 2. Numerical finite element model in ABAQUS/Standard; bending is applied about the x-axis and symmetry in the yz-plane is considered.

material response more accurately, certain amendments to the original form of the constitutive model proposed in (Armstrong and Frederick, 1966) are required. Herein, a modification of the model is adopted, based on the proposal of Ucak and Tsopelas (2011), defining a “critical strain level” at the end of the plastic plateau ε_{qcr} , and adjusting the hardening parameter C so that it represents either the plastic plateau or the Bauschinger effect. More details of the constitutive model are offered in (Chatzopoulou et al., 2016). The above material model has been implemented through a user-subroutine (UMAT) in ABAQUS/Standard, using an “elastic predictor – plastic corrector” (Euler-backward) numerical integration scheme (Chatzopoulou et al., 2016).

The material model is calibrated through a uniaxial stress-strain curve shown in Fig. 3. The yield stress of steel material σ_Y is equal to 498 MPa (72 ksi). A similar curve has been reported in (Herynk et al., 2007) for an X-70 grade steel.

3. Numerical results for cyclic bending process

During the reeling procedure the pipe is subjected to spooling, unspooling and straightening, which induce bending strains (ε_B) well into the plastic range of the steel material. In Fig. 4 the reeling process is schematically described in terms of the corresponding

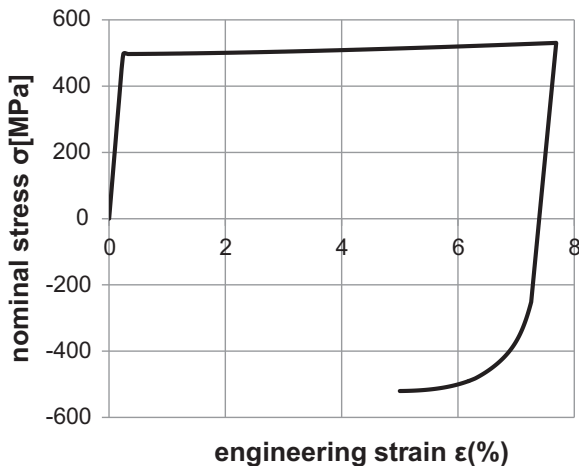


Fig. 3. Material curve of steel grade X-70 under initial plastic loading and reverse loading.

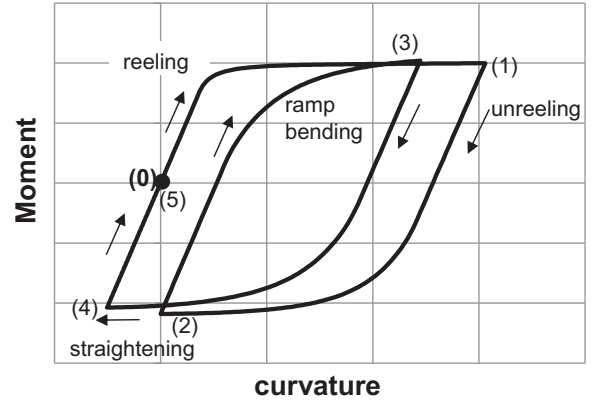


Fig. 4. Schematic representation of the five consecutive loading steps of the pipe during the reeling process.

moment-curvature diagram; the following steps can be identified:

Step 1 (0 → 1): The pipe is plastically bent up to curvature k_1 , corresponding to maximum strain of approximately 2%, corresponding to spooling of the pipe onto the reel at the initial stage.

Step 2 (1 → 2): The pipe undergoes unspooling and straightening, so that its curvature becomes zero ($k_2 = 0$).

Step 3 (2 → 3): The pipe is subjected to bending up to curvature k_3 in the initial bending direction as it passes over the ramp.

Step 4 (3 → 4): The pipe is straightened again and bent reversely to curvature (k_4). The maximum reverse bending curvature is carefully selected to result in straight configuration when bending loading is released (see next step).

Step 5 (4 → 5): The pipe is unloaded reaching a straight configuration, corresponding to zero moment curvature ($M_5 = 0$ and $k_5 = 0$).

In the present analysis, the five aforementioned loading steps are applied on three different pipes. The pipes have the same outer diameter D (323.85 mm), whereas thickness is equal to 23.82 mm (0.93 in), 19.05 mm (0.75 in) and 15.24 mm (0.6 in); they are denoted as pipe I, pipe II and pipe III respectively.

Three different cyclic load cases are considered. In the first case (case 1), during the first step, a value of curvature is applied corresponding to a local tensile longitudinal strain equal to 2% on the pipe wall at point A located on the outer surface of the pipe extrados (see Fig. 2). The same curvature is applied during the third step ($k_3 = k_1$). In the second case (case 2), the initially applied curvature k_1 corresponds to a strain equal to 1% at point A, and curvature k_3 is equal to k_1 . In the third case (case 3), curvature k_1 corresponds to tensile longitudinal strain equal to 2% strain, while curvature k_3 corresponds to 1.6% local strain at point A.

The three load cases are applied on pipe II to examine the effect of cyclic bending amplitude on pipe material and ovalization. In the first case, during the first step, the value of curvature is equal to $k_1 = 0.6t/D_m^2$, where D_m is the mean pipe diameter and t is pipe thickness ($D_m = D - t$), corresponding to a local tensile longitudinal strain equal to 2% at point A. The same curvature is applied during the third step ($k_3 = k_1$). In the second case, the value of initially applied curvature k_1 is equal to $0.3t/D_m^2$, corresponding to tensile strain equal to 1% at point A, and k_3 is equal to k_1 . In the third case, curvature k_1 is equal to $0.6t/D_m^2$ (2% strain at point A), while curvature k_3 is equal to $0.48t/D_m^2$ corresponding to 1.6% local strain. The above applied curvature values at each loading stage are summarized in Table 1. In the numerical results shown in the following sections, the values of pressure P , moment M and curvature k are normalized by the yield pressure $P_y = 2\sigma_Y t/D_m$, the fully plastic moment $M_0 = \sigma_Y D_m^2 t$, and the curvature parameter $k_l = t/D_m^2$ respectively.

In Fig. 5, Fig. 6 and Fig. 7, the moment-curvature diagrams for

Table 1
Value of applied curvatures k_1 and k_3 for each cyclic load case for pipe II.

Cyclic load case	Applied curvature	
	k_1/k_I	k_3/k_I
1	0.60	0.60
2	0.30	0.30
3	0.60	0.48

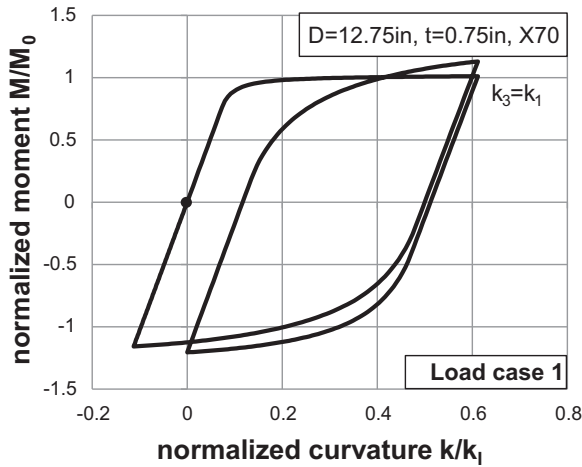


Fig. 5. Moment-curvature diagrams for cyclic load case 1 (pipe II).

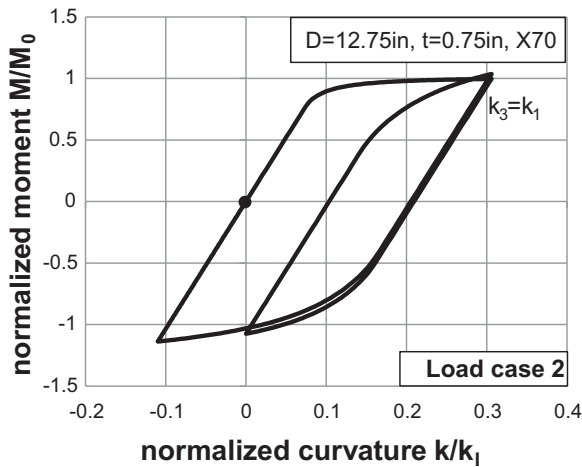


Fig. 6. Moment-curvature diagrams for cyclic load case 2 (pipe II).

each cyclic load case for pipe II ($D/t = 17$) are depicted. Furthermore, Figs. 8–10 show the axial stress-strain path, in the outer surface of the pipe extrados (point A in Fig. 2) obtained by the cyclic loading process. The final value of stress (residual stress) at point A, after the two bending cycles, is nearly 200 MPa for all three cyclic load cases, which is approximately 40% of yield stress. At the point opposite of A (intrados of bent pipe) the residual stress is nearly -200 MPa. Fig. 11 shows the distribution of residual axial and circumferential stress for cyclic load case 1. The results indicate that the residual circumferential stresses are smaller than the residual axial stresses.

Moreover, load case 1 is applied on pipes I and III. Fig. 12–15 illustrate the moment-curvature paths for the pipe I and pipe III (D/t equal to 13.59 and 21.25 respectively) and the stress-strain path in the axial direction, at the tension side of pipe outer surface.

The material behavior is considered initially isotropic, which is a reasonable assumption based on previous observations in

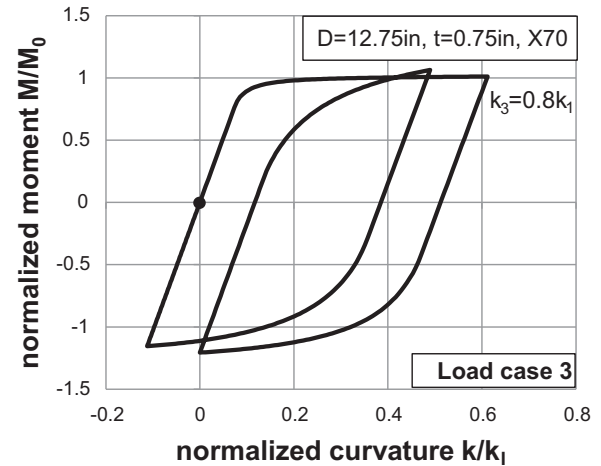


Fig. 7. Moment-curvature diagrams for cyclic load case 3 (pipe II).

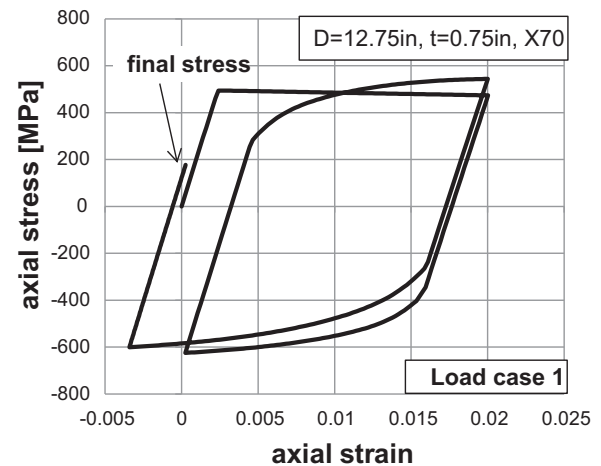


Fig. 8. Stress-strain path at point A for cyclic load case 1 (pipe II).

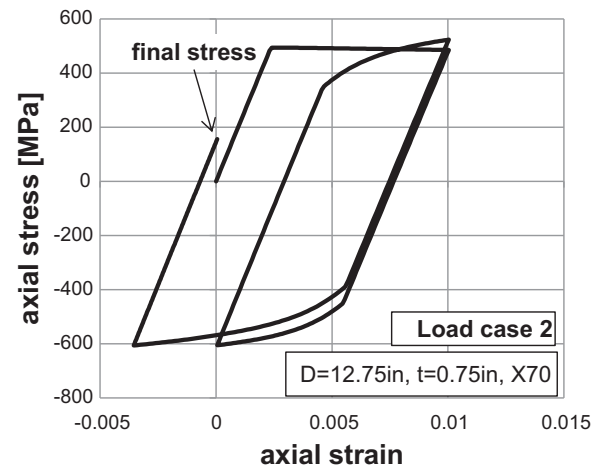


Fig. 9. Stress-strain path at point A for cyclic load case 2 (pipe II).

seamless steel pipes. Nevertheless, due to cyclic plastic loading, the mechanical properties of the virgin material are influenced and material anisotropy is induced, which can be an important factor for the mechanical behavior and the ultimate capacity of offshore pipes under external pressure. In practice, steel material anisotropy at the end of the reeling process can be evaluated by extracting strip specimens from the pipe at critical locations

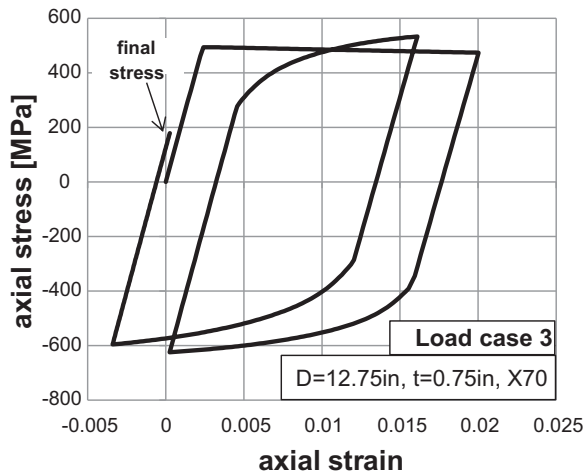


Fig. 10. Stress-strain path at point A for cyclic load case 3 (pipe II).

(intrados or extrados) in the longitudinal and hoop direction. Subsequently, the strip specimens are subjected to uniaxial tension, in the longitudinal direction and compression in the circumferential (hoop) direction, and the corresponding stress-strain curves in each direction are obtained. It is noted that the compressive material behavior should be examined in the hoop direction, because it is related to the pipeline buckling resistance against external pressure.

A numerical simulation of the above procedure is conducted in the present study. More specifically, a specific integration point is selected at a critical location (e.g. point A at the extrados). Throughout the simulation of cyclic bending, all material state parameters (stresses, strains) are recorded at this integration point. Subsequently, a “unit cube” finite element model is considered, and the material parameters from the selected integration point are introduced as initial state variables in this model. A first analysis step with zero external loading is performed, simulating the extraction of the strip specimen from the pipe. Subsequently, a second loading step is performed, where the “unit cube” is loaded under uniaxial compression in the pipe hoop direction, or under uniaxial tension in the direction parallel to the pipe axis, and the corresponding stress-strain paths are obtained. Assuming that the

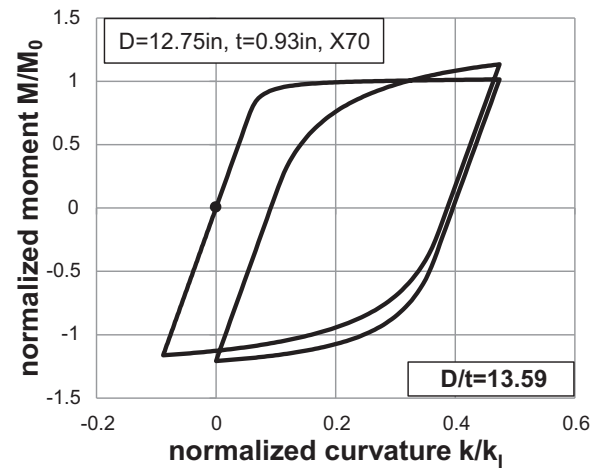


Fig. 12. Moment-curvature diagram for pipe I ($D/t = 13.59$).

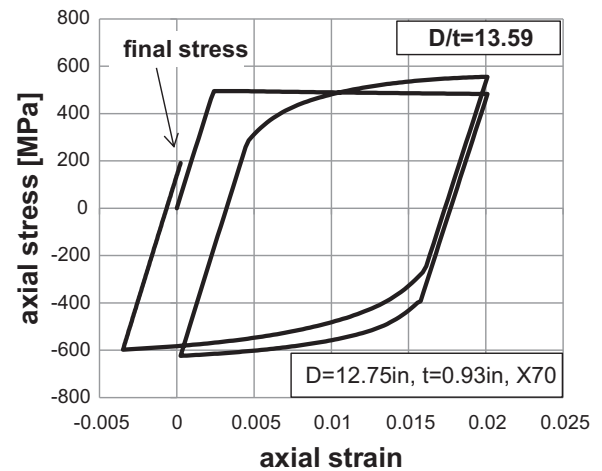


Fig. 13. Stress-strain path at point A for pipe I ($D/t = 13.59$).

axial response represents the fundamental response of pipe material, the different behavior in the hoop direction is quantified in

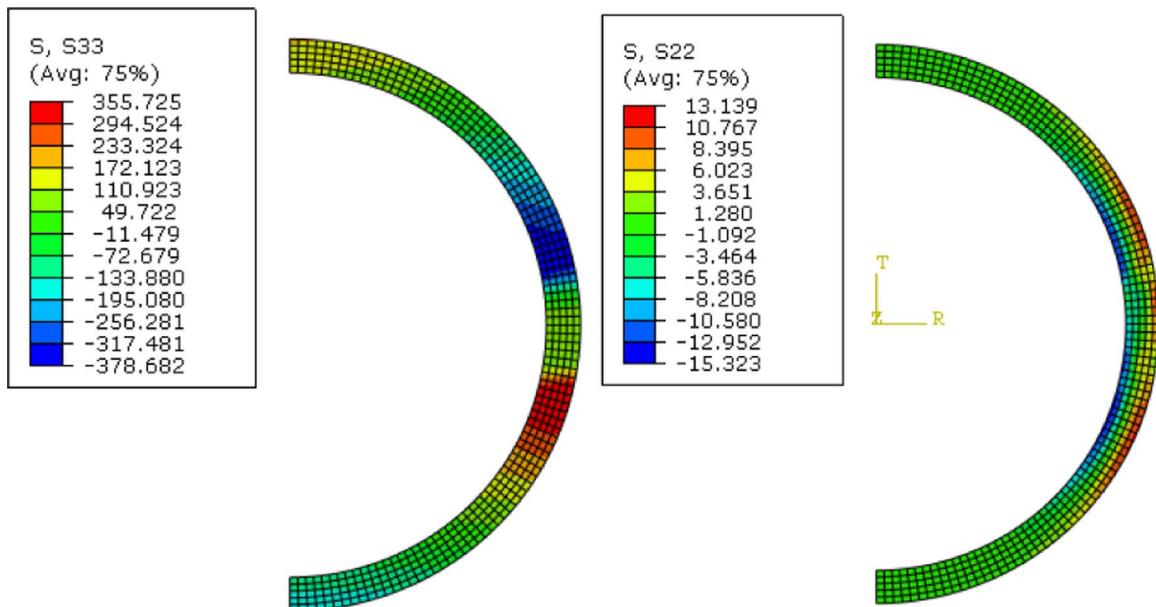


Fig. 11. Distribution of residual (axial and circumferential) stresses after for cyclic load case 1 (pipe II $D/t = 17$).

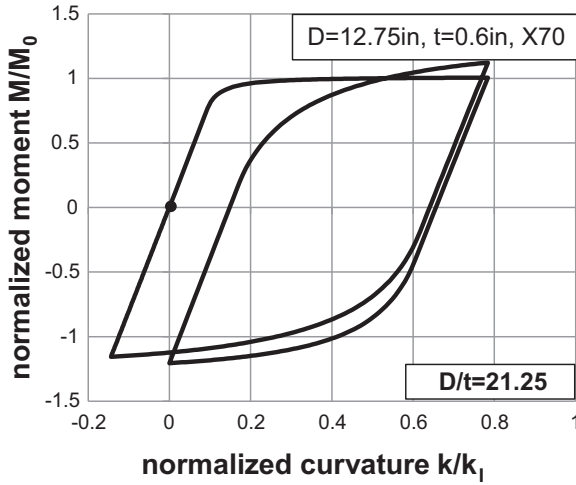


Fig. 14. Moment-curvature diagrams for pipe III ($D/t = 21.25$).

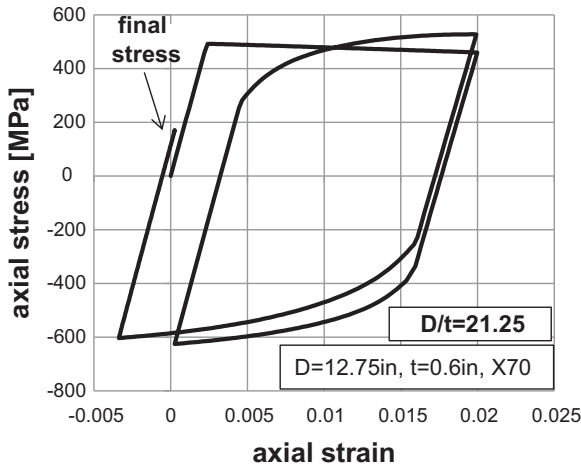


Fig. 15. Stress-strain path at point A for pipe III ($D/t = 21.25$).

terms of the following anisotropy parameter:

$$S = \frac{\sigma_{Y\theta}}{\sigma_{YX}} \quad (3)$$

where σ_{YX} is the tensile yield stress in the pipe axial direction and $\sigma_{Y\theta}$ is the compressive circumferential yield stress of pipe material.

Figs. 16–18 depict the uniaxial stress-strain material response of pipe II at the critical location A (shown in Fig. 2) in the longitudinal and hoop direction for the three load cases indicating material anisotropy in the two principal directions of the pipe. The results show that anisotropy increases with increasing initial strain during cyclic loading. Maximum reeling-induced anisotropy has been observed in load case 1 (14%, or $S = 1.14$). Furthermore, the anisotropy induced in pipes I and III (D/t equal to 13.59 and 21.25 respectively) show a similar anisotropy level, independent of the value of the D/t ratio.

An important geometric parameter for assessing the mechanical behavior of deep offshore pipes, subjected to external pressure, is the ovalization of the pipe cross-section, also referred to as “cross-sectional ovality”. It is often expressed by the following ovalization parameter Δ (Kyriakides and Corona, 2007; Murphy and Langner, 1985; API RP 1111, 1999):

$$\Delta = \frac{|D_1 - D_2|}{D_1 + D_2} \quad (4)$$

where D_1 and D_2 are the maximum and minimum outer pipe

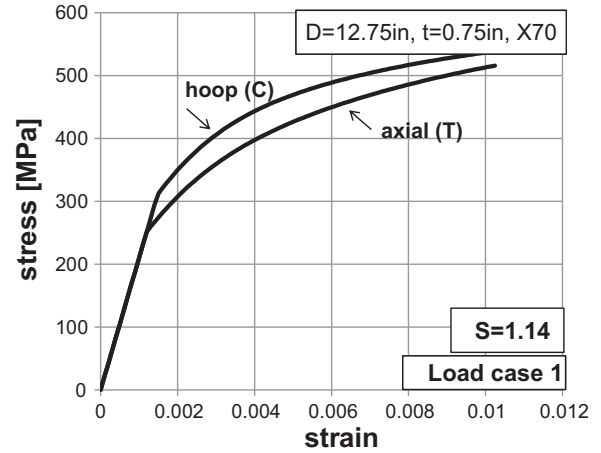


Fig. 16. Comparison of the axial tensile (T) and circumferential (hoop) compressive (C) stress-strain curves for cyclic load case 1.

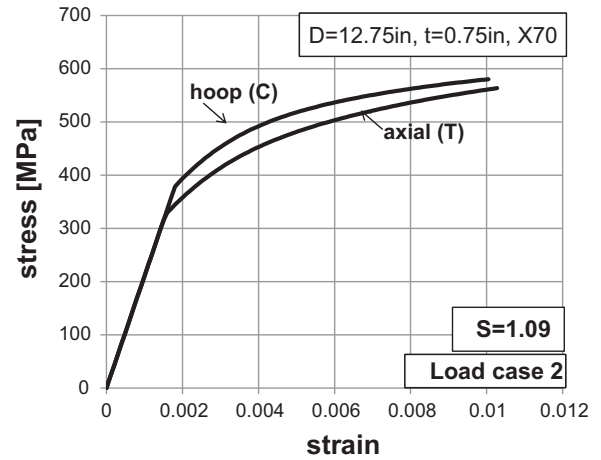


Fig. 17. Comparison of the axial tensile (T) and circumferential compressive (C) stress-strain curves for cyclic load case 2.

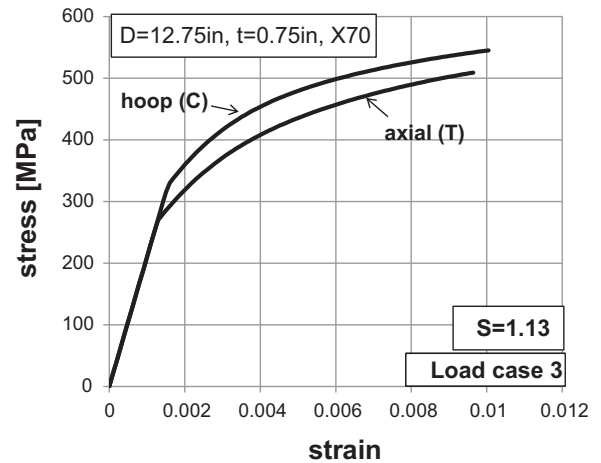


Fig. 18. Comparison of the axial tensile (T) and circumferential compressive (C) stress-strain curves for cyclic load case 3.

diameter respectively. In the present study, initial ovalization denoted as Δ_0 is the ovalization after the manufacturing process (“as received” pipe), while the ovalization Δ_{0a} is the residual ovalization after reeling. The latter constitutes an initial geometric imperfection for the reeled pipe, which can affect the ultimate capacity under external pressure during deep water installation, causing

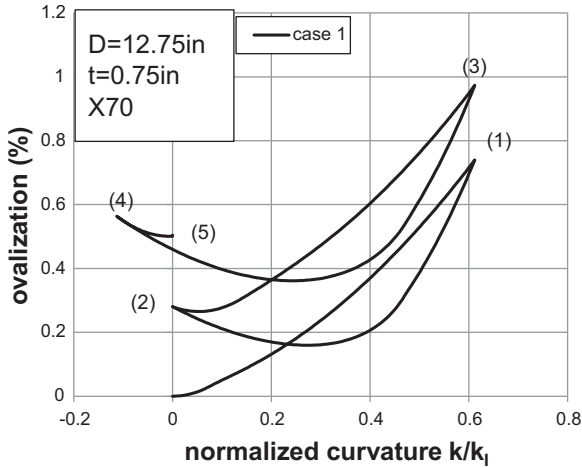


Fig. 19. Evolution of cross-sectional ovalization during cyclic loading of pipe II (case 1).

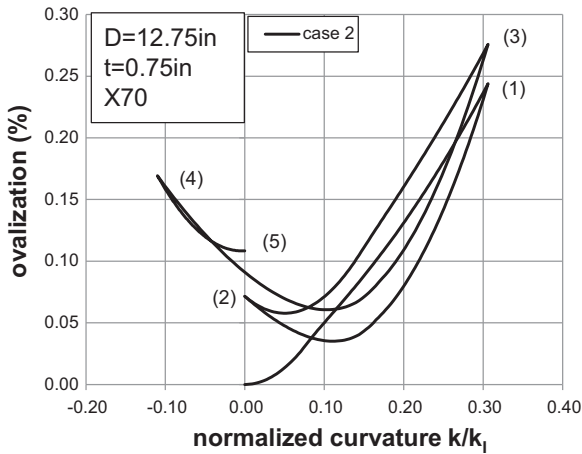


Fig. 20. Evolution of cross-sectional ovalization during cyclic loading of pipe II (case 2).

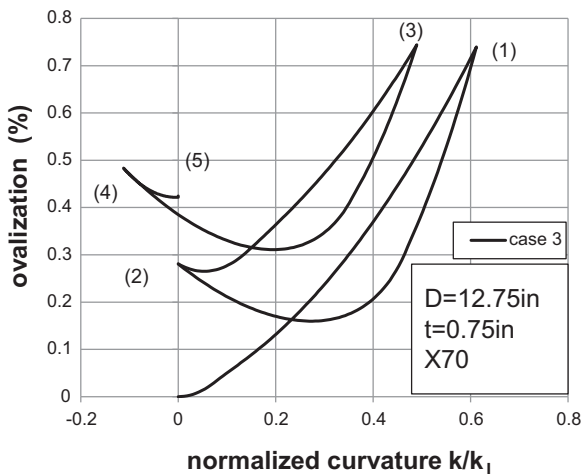


Fig. 21. Evolution of cross-sectional ovalization during cyclic loading of pipe II (case 3).

premature collapse and will be examined in the next section. In Fig. 19, Fig. 20 and Fig. 21 the evolution of ovalization is illustrated for the three cyclic load cases. The results show that the maximum ovalization developed during the cyclic loading process may be quite significant and may reach a value of 1% at the end of loading

stage 3. On the other hand, the residual (remaining) value of ovalization at stage (5), i.e. at the end of cyclic loading process, is substantially less than the maximum value. For case 1, the residual ovalization Δ_{0a} is equal to 0.5% while for case 2 and 3 the values residual ovalization values Δ_{0a} are 0.11% and 0.42% respectively.

Furthermore, the effect of the D/t value on the value of residual ovalization is examined. The three pipes under consideration are subjected to cyclic loading with corresponding local tensile longitudinal strain equal to 2% and the ovalization throughout the analysis is recorded. The residual ovalization Δ_{0a} is computed equal to 0.83% for pipe III, which is significantly different compared to the value of 0.26% for pipe I, and indicates that the residual ovalization increases with increasing the value of the D/t ratio. The residual ovalization values are well below 1.5%, which is a maximum value imposed by DNV-OS-F101 (DNV OS-F101, 2012). Note that the ovalization measure Δ defined in Eq. (4) is half the one defined by the DNV rules (DNV OS-F101, 2012).

4. Structural behavior of pipes after reeling

During deep offshore installation, which follows reeling and unreeling, the pipe experiences a combination of external pressure and bending loading. The purpose of the present analysis is to quantify the effect of the cyclic bending process on the mechanical response and the ultimate capacity of the pipe, subjected to (a) external pressure, and (b) pressurized bending conditions.

4.1. Mechanical behavior under external pressure

The three cases of Table 1 are considered, using the finite element model described in Section 2. The numerical simulation consists of sequence of six loading steps. The first five steps correspond to the two bending cycles of reeling (as described in the previous section), followed by a step where external pressure is applied using a Riks continuation algorithm, capable of describing efficiently buckling and post-buckling behavior.

In Fig. 22, the collapse pressure of pipe II, denoted as P_{CO} , is shown for each cyclic loading case; this is the maximum pressure sustained by the pipe. The numerical results indicate that for a specific pipe and for increasing level of maximum bending strain (i.e. the value of curvature k_1), the collapse pressure decreases. In addition, the comparison of Case 1 with Case 3 shows that the lower value of k_3 in Case 3 results to a slightly higher pressure capacity of the pipe. The observed behavior can be directly

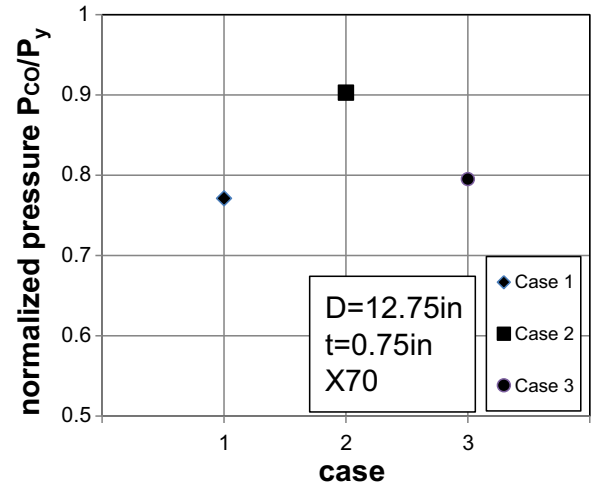


Fig. 22. Ultimate capacity of "reeled" pipe II under external pressure for the three load cases.

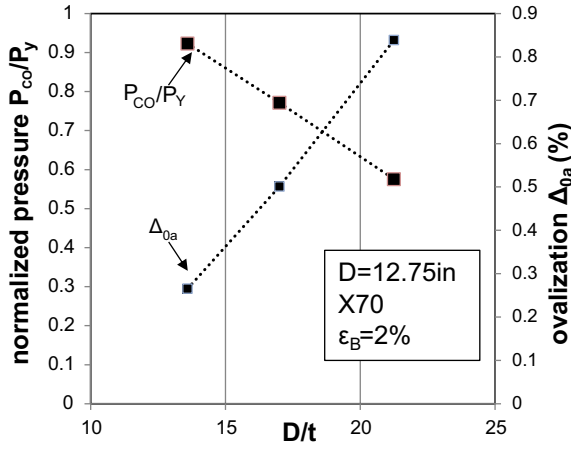


Fig. 23. Pressure capacity and residual ovalization after cyclic bending for the three pipes under consideration.

correlated to the residual cross-sectional ovalization of the pipe at the end of cyclic bending process, shown in Fig. 19, Fig. 20 and Fig. 21. More specifically, Case 2 induces less residual ovalization (Fig. 20) than in Case 1 and Case 3, resulting in higher external pressure capacity, as shown in the results of Fig. 22.

Moreover, the effect of the D/t value on the pressure capacity of reeled pipes is examined, by comparing the analysis results for pipes I and III. The value of the D/t ratio affects the value of residual ovalization (Δ_{0a}) and therefore, it is expected to affect the pressure capacity of the reeled pipes. Fig. 23 verifies that external pressure capacity decreases with increasing value of the D/t ratio.

To analyze further the effect of cyclic loading on external pressure capacity, a comparison between reeled and unreeled pipes has been conducted, considering pipes with four different D/t ratios and initial ovalization Δ_0 equal to 0.2% (ovalization of the as-received pipe). Furthermore, two sets of unreeled pipes are considered with material, diameter and thickness identical to the ones of the pipes examined in the previous section. The first set of pipes, denoted as “unreeled A”, has an initial ovalization Δ_0 equal to 0.2%. The second set of pipes (“unreeled B” as described in Section 3) has initial ovalization equal to Δ_{0a} , i.e. the ovalization of the pipes after the reeling (cyclic bending) process. Both unreeled pipes A and B are stress free. Fig. 24 shows the pressure capacity of reeled and unreeled pipes. The results indicate that unreeled pipes

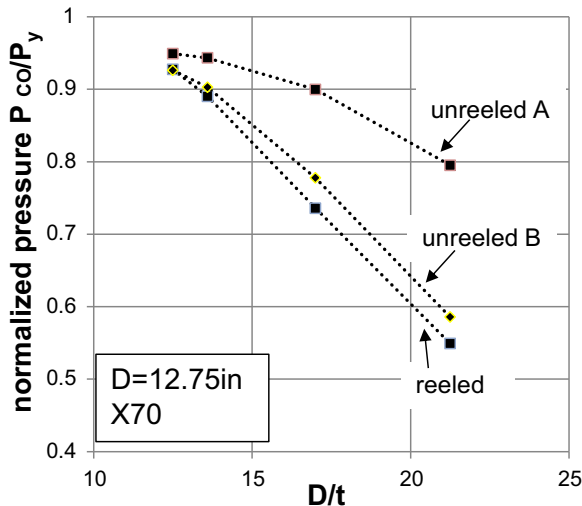


Fig. 24. Pressure capacity in terms of the four D/t values considered for reeled and unreeled pipes.

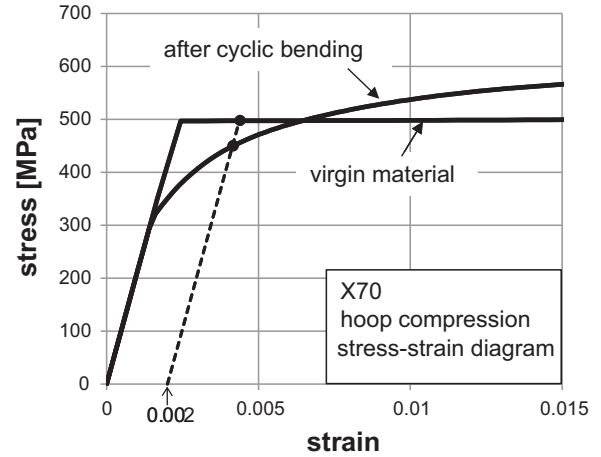


Fig. 25. Comparison of virgin material uniaxial response with circumferential compressive stress-strain curve after cyclic bending.

of type A have higher pressure capacity than the corresponding reeled pipes and that as the value of D/t , increases the difference between the pressure capacity of reeled and unreeled pipes increases. The present results are in complete agreement with the previous study of Pasqualino et al. (2004). Furthermore, unreeled pipes (unreeled B) have higher pressure capacity than reeled pipes as shown in Fig. 24. This is attributed to the fact that the compression yield stress of the reeled pipe in the hoop the direction (governing the pressure capacity) is lower than the yield stress of the intact pipe as shown in Fig. 25.

4.2. Effect of reeling on pressurized bending capacity

During deep-water pipeline installation, at the “sagbend” region (Fig. 1), the pipe is subjected to bending in the presence of high external pressure, which constitutes an important stage of offshore pipeline design (Kyriakides and Corona, 2007). Bending introduces cross-sectional ovalization, which is accentuated by the presence of external pressure, resulting in premature collapse of the pipe (Corona and Kyriakides, 1988; Karamanos and Tassoulas, 1991).

To analyze this interaction, an appropriate loading pattern is considered in the finite element model, through an appropriate sequence of loading steps: cyclic loading is applied first in five consecutive steps, as described above; subsequently uniform external pressure is raised up to a certain level and, finally, keeping the external pressure constant, a final bending step is applied until a limit (maximum) M_{max} moment is reached, using Riks continuation algorithm.

The value of bending curvature k_{max} corresponding to the maximum bending moment M_{max} during the final loading step is referred to as “critical curvature”, and is an important parameter for offshore pipe design (Kyriakides and Corona, 2007). In the case of thick-walled pipes, which are candidates for deep-water applications, bending response is governed by limit moment instability due to ovalization, and the value of k_{max} defines the rotational capacity of the pipe. For each cyclic-loading case of Table 1, pressurized bending is considered, with the loading sequence described above and the results are depicted in Fig. 26, in the form of pressure-curvature interaction diagrams. For the purpose of consistency with the physical problem shown in Fig. 1, bending load is applied about the x-axis, but in the opposite direction to the one during reeling (i.e. opposite to the one shown by the moment vector in Fig. 2). Fig. 27 shows the moment-curvature diagrams in the presence of external pressure equal to 20% of nominal yield pressure P_y , for the three cyclic load cases. On each

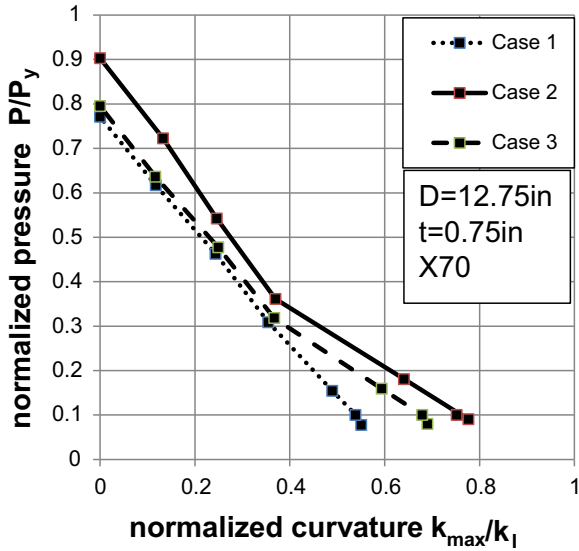


Fig. 26. Pressure-curvature interaction diagram ($P \rightarrow \kappa$) for three cyclic load cases.

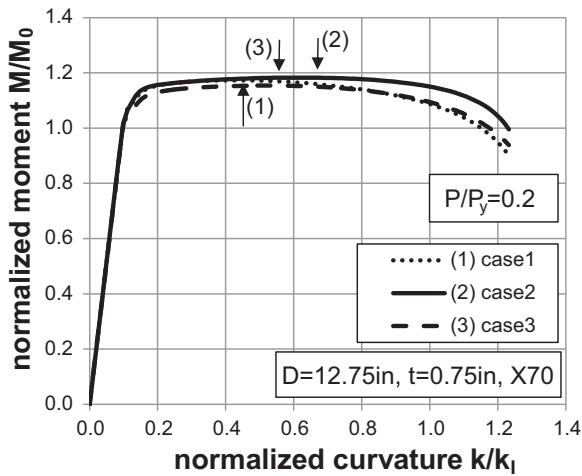


Fig. 27. Bending response (moment-curvature diagrams) for the three cyclic load cases of pipe II; external pressure is equal to 20% of P_y .

diagram, the location corresponding to maximum bending moment is denoted with arrow (1) or (↑). The results show that the pipes reeled with load cases 1 and 3 have a similar bending capacity, whereas the pipe subjected to cyclic bending of case 2 exhibits slightly higher bending capacity. This result is attributed to the fact that in case 2 the pipe is subjected to maximum tensile strain of only 1%, which induces less plastic deformation and smaller cross-sectional ovalization than the other two cyclic load cases.

To analyze further the effect of cyclic loading on pressurized bending capacity, comparison between reeled and unreeled pipes is performed. A pipe with material and geometric (thickness, diameter) properties similar to pipe II ($D/t = 17$) is considered, assuming initial ovalization Δ_0 equal to 0.2% (ovalization of the as-received pipe), subjected to cyclic bending prior to the application of pressure and bending, referred to as “reeled”. Furthermore, two unreeled pipes with similar properties are considered, as in the previous section; the first unreeled pipe, denoted as “unreeled A”, has the same initial ovalization Δ_0 equal to 0.2%. The second pipe (“unreeled B”) has an initial ovalization equal to Δ_{0a} , i.e. the ovalization obtained after the reeling process. It should be noted that unreeled pipes A and B are considered stress-free before the

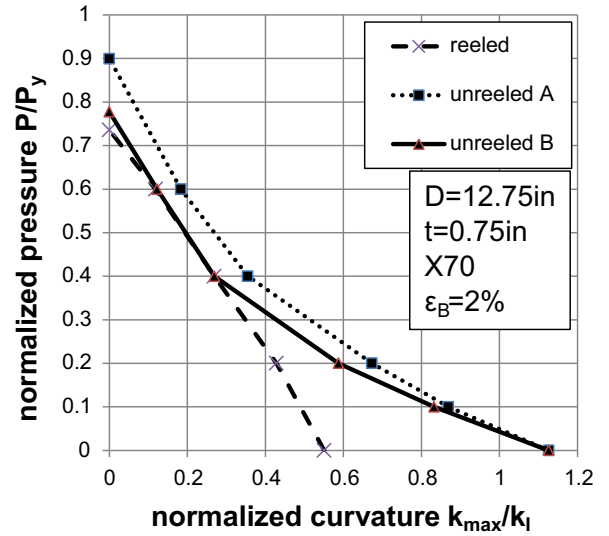


Fig. 28. Pressure-curvature ($P \rightarrow \kappa$) interaction diagram for reeled and unreeled pipes.

application of pressure and bending. Fig. 28 shows the interaction diagram ($P \rightarrow k$) for the “reeled” and the two “unreeled” pipes. The results show that unreeled A pipe has greater capacity than the reeled pipe. Unreeled B pipe has the same capacity with the reeled pipe for high values of pressure and the same response as with unreeled A for low pressure levels. This is attributed to the fact that, for high levels of pressure, pipe ovalization is the governing factor for the ultimate capacity; therefore unreeled B and reeled pipes have similar responses because they have the same initial ovalization before external pressure is applied. On the other hand, for low values of pressure, residual stresses constitute the dominant parameter; therefore unreeled A and unreeled B pipes, which have similar geometry and are both residual stress free, exhibit similar response. Fig. 29 and Fig. 30 depict the corresponding moment-curvature diagrams in the presence of external pressure equal to 10% and 20% of P_y respectively. The results indicate that the reeled pipe is capable of reaching higher bending moment values than the two unreeled pipes. It should be noted that, at low pressure levels, the moment-curvature diagram upon initial yielding is nearly flat, so that the value of k_{max} corresponding to the maximum value of bending moment may not be a reliable measure of bending capacity.

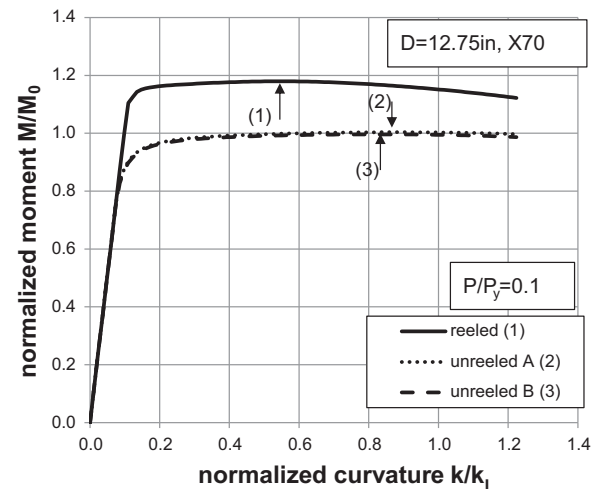


Fig. 29. Bending response (moment-curvature diagrams) for reeled and unreeled pipes; external pressure equal to 10% of P_y .

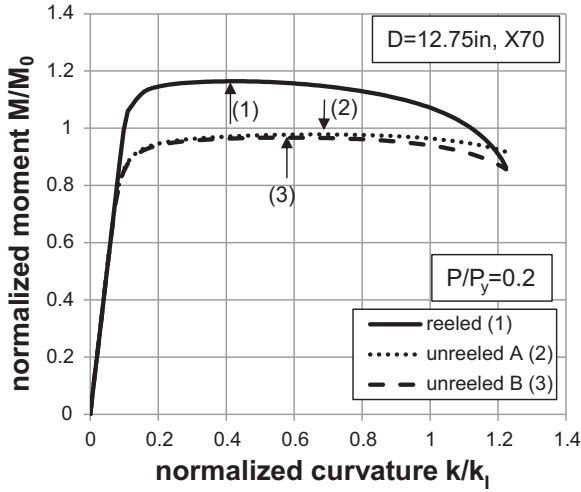


Fig. 30. Bending response (moment-curvature diagrams) for reeled and unreeled pipes; external pressure equal to 20% of P_y .

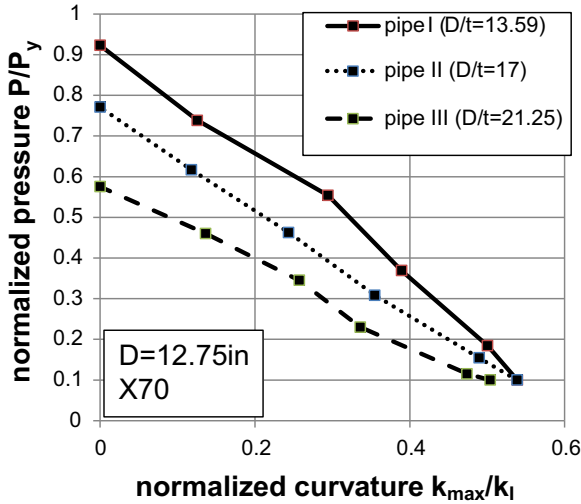


Fig. 31. Pressure-curvature ($P \rightarrow \kappa$) interaction diagram for pipes I, II and III.

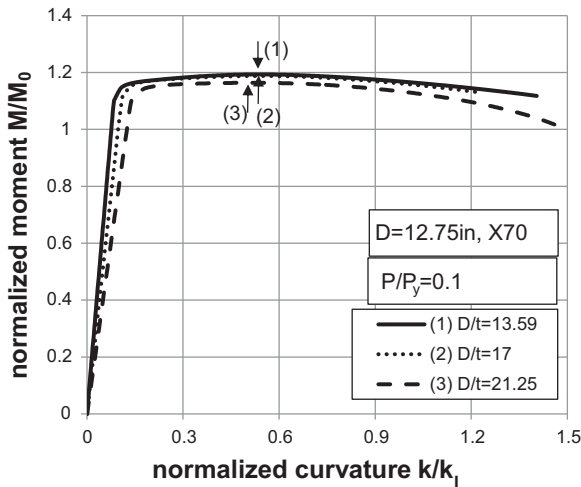


Fig. 32. Bending response (moment-curvature diagrams) for pipes I, II and III; external pressure equal to 10% of P_y .

Furthermore, in Fig. 31 the pressure-curvature interaction diagrams of pipes I, II and III without initial ovalization Δ_0 are presented in normalized form. Pipe I has the smallest D/t value, and therefore, its cross-section is stiffer and less susceptible to structural instability due to ovalization. Therefore, it has higher bending capacity than the other two pipes. Fig. 32 shows the corresponding moment-curvature diagrams in the presence of external pressure at 10% of the yield pressure. For this low pressure level, small differences on the value of k_{\max} are observed.

Furthermore, comparison of the present results is conducted with an empirical interaction formula, introduced by Murphey and Langner (Murphey and Langner, 1985) and referred to as “Shell equation”, also adopted by the API specification (API RP 1111, 1999), and widely used in offshore pipeline design. The equation assumes a linear interaction between the level of pressure P and the bending curvature κ_{\max} , as follows:

$$\frac{P}{P_c} + \frac{\kappa_{\max}}{\kappa_b} = g(\Delta) \quad (5)$$

In Eq. (5), $g(\Delta) = (1 + 20\Delta)^{-1}$ is a function of the ovalization amplitude Δ , $\kappa_b = t/D^2$ is an estimate of the buckling curvature under zero pressure (D is the outer pipe diameter), P_c is an estimate of the ultimate external pressure sustained by the pipe, given by the following equation

$$P_c = \frac{P_p P_e}{\sqrt{P_p^2 + P_e^2}} \quad (6)$$

where the plastic pressure P_p and the elastic buckling pressure P_e are defined as follows:

$$P_p = 2\sigma_y \frac{t}{D} \quad (7)$$

and

$$P_e = \frac{2E}{1 - \nu^2} \left(\frac{t}{D} \right)^3 \quad (8)$$

The comparison is shown in Figs. 33–35 for pipes I, II and III. In Eq. (5), the ovalization Δ is considered equal with the residual ovalization Δ_{0a} after the reeling process. The comparison for all three pipes shows that for high values of pressure the empirical equation provides good, yet somewhat conservative estimates for the bending curvature, while for low values of pressure the empirical equation overestimates the bending deformation capacity.

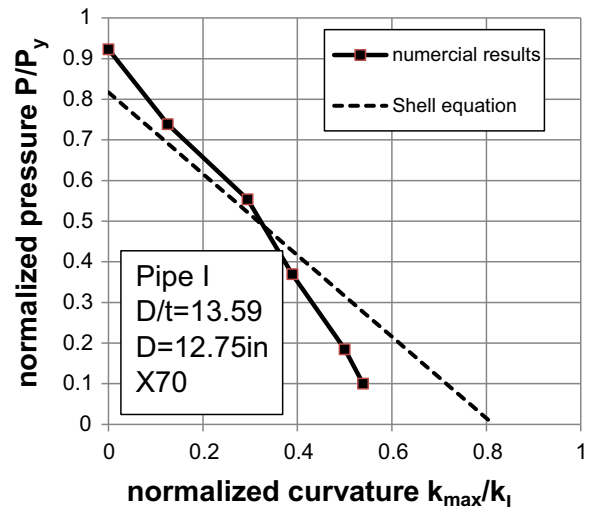


Fig. 33. Pressure-curvature ($P \rightarrow \kappa$) interaction diagram for pipe I; Shell equation and numerical results.

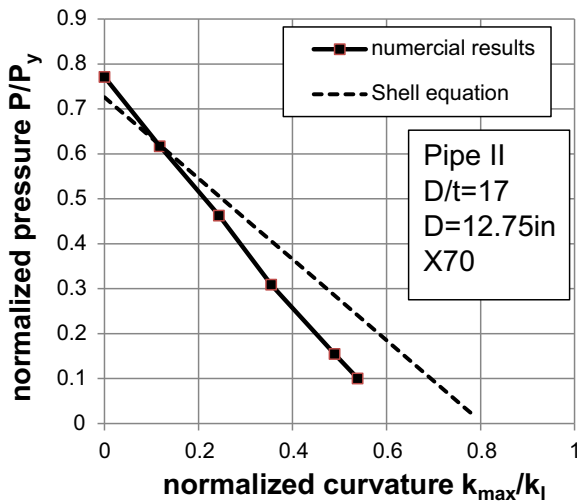


Fig. 34. Pressure-curvature ($P \rightarrow \kappa$) interaction diagram for pipe II; Shell equation and numerical results.

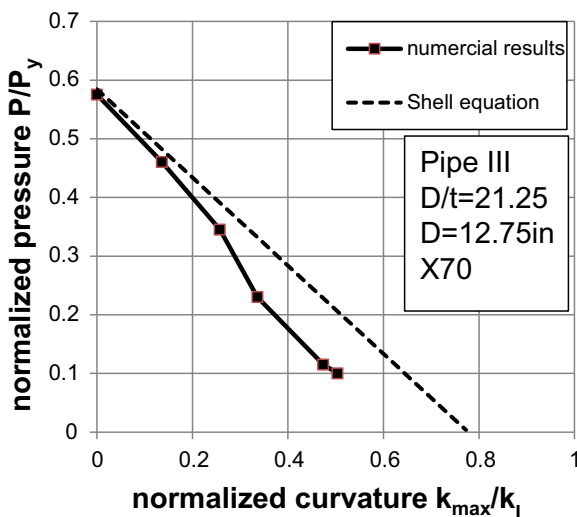


Fig. 35. Pressure-curvature ($P \rightarrow \kappa$) interaction diagram for pipe III; Shell equation and numerical results.

This is attributed to the fact that this empirical equation does not take into account the residual stresses induced by cyclic bending, which is a dominant factor for bending response under low values of external pressure.

5. Conclusions

Motivated by the reeling installation method, the effect of initial cyclic bending loading on the material properties of thick-walled steels seamless pipes with D/t values between 13.59 and 21.25 are examined using finite element simulation tools. In addition, the effects of cyclic bending on the mechanical behavior of those pipes subjected to external pressure and bending are investigated. A quasi-two dimensional numerical approach has been developed, adopting an advanced constitutive material model, introduced by the authors elsewhere, capable of describing the main features of elastic–plastic material behavior, and implemented within the finite element model through a material-user subroutine. In the first part of the paper, pipe cyclic bending conditions are simulated for three characteristic cases, representing the reeling process. Subsequently, a parametric analysis is conducted, focusing on the effects of cyclic bending due to reeling on the ultimate capacity of

the pipe, under external pressure and pressurized bending loading conditions.

The numerical results show that a seamless pipe, which is considered initially isotropic, exhibits material anisotropy features when subjected to cyclic plastic bending. Furthermore, cross-sectional ovalization at the end of the cyclic bending process is a decisive parameter for the external pressure capacity of the pipe. Higher values of bending strain (curvature), induced by the cyclic bending process, result in increased pipe ovalization and, consequently, in reduced external pressure capacity. In addition, pressure-curvature interaction diagrams have been developed for three cyclic bending cases, showing that higher values of cyclic-bending strain reduces the capacity of pipe in resisting the deep-water installation loads.

The behavior of “reeled” pipes (with maximum local strain ϵ_B equal to 2%) and “unreeled” pipes is compared. Reeled pipes have very similar external pressure capacity with unreeled pipes having initial ovalization equal to the residual ovalization of reeled pipes. They also have similar bending capacity under high external pressure levels. However, at low values of external pressure they behave differently; reeled pipes are capable of reaching higher bending moment values than unreeled pipes, but the corresponding curvature capacity of reeled pipes is lower. The effect of the D/t value on pressure and bending capacity of reeled pipes is also examined, showing that severe cyclic bending (tensile strain ϵ_B equal to 2%) has a more pronounced effect on pressure and bending capacity in pipes with higher D/t ratio.

Furthermore, the numerical results are compared with an empirical equation, widely used in pipeline design, indicating an over-prediction of bending deformation capacity for low values of external pressure. Finally, the values of residual ovalization induced by cyclic bending are well below the threshold ovalization value imposed by the relevant DNV pipeline standard.

References

- API RP 1111, 1999. Design, Construction, Operation and Maintenance of Offshore Hydrocarbon Pipelines (Limit State Design), Washington, DC.
- Armstrong, P. J., Frederick, C. O., 1966. A mathematical representation of the multiaxial Bauschinger effect, CEBG Report No. RD/B/N 731.
- Brown, G., Tkaczyk, T., Howard, B., 2004. Reliability Based Assessment of Minimum Reelable Wall Thickness for Reeling. In: Proc. of the International Pipeline Conference, Alberta, Canada.
- Chatzopoulou, G., Karamanos, S.A., Varelis, G.E., 2016. Finite element analysis of UOE manufacturing process and its effect on mechanical behavior of offshore pipes. *Int. J. Solids Struct.* 83, 13–27.
- Corona, E., Kyriakides, S., 1988. On the collapse of inelastic tubes under combined bending and pressure. *Int. J. Solids Struct.* 24, 505–535.
- Dawood, A., Kenny, S., 2013. Finite Element Method Simulating the Pipeline Mechanical Response During Reel Lay Installation. In: Proc. of the 32th International Conference on Offshore Mechanics and Arctic Engineering, Nantes, France.
- DNV OS-F101, 2012. Submarine Pipeline Systems, Det Norske Veritas, Oslo, Norway.
- Heier, E., Østby, E., Akselsen, O. M., 2013. Reeling Installation of Rigid Steel Pipelines at Low Temperature. In: Proc. Of the 23rd International Offshore and Polar Engineering, Anchorage, Alaska, USA.
- Herynk, M.D., Kyriakides, S., Onoufriou, A., Yun, H.D., 2007. Effects of the UOE/UOC pipe manufacturing processes on pipe collapse pressure. *Int. J. Mech. Sci.* 49, 533–553.
- Karamanos, S.A., Tassoulas, J.L., 1991. Stability of inelastic tubes under external pressure and bending. *J. Eng. Mech.* 117 (12), 2845–2861.
- Kyriakides, S., Corona, E., 2007. *Mechanics of Offshore Pipelines, Buckling and Collapse Vol. 1*. Elsevier.
- Kyriakides, S., Liu, Y., 2014. Effect of geometric and material discontinuities on the reeling of pipelines. In: Proc. of the 33th International Conference on Offshore Mechanics and Arctic Engineering, San Francisco, California.
- Manouchehri, S., Howard, B., Denniel, S., 2008. A Discussion of the Effect of the Reeled Installation Process on Pipeline Limit States. In: Proc. of the 18th International Offshore and Polar Engineering Conference, Vancouver, Canada.
- Martinez, M., Brown, G., 2005. Evolution of pipe properties during reel-lay process: experimental characterisation and finite element modeling. In: Proc. of the 24th International Conference on Offshore Mechanics and Arctic Engineering, Halkidiki, Greece.

- Meiwes, K. C., Höhler, S., Erdelen-Peppler, M., Brauer, H., 2014. Full-scale reeling tests of HFI welded line pipe for offshore reel-laying installation. In: Proc. of the 2014 10th International Pipeline Conference, Calgary, Alberta, Canada.
- Meiwes, K. C., Erdelen-Peppler, M., Brauer, H., 2014. Impact of small-scale reeling simulation on mechanical properties on line pipe steel. In: Proc. of the 2014 10th International Pipeline Conference, Calgary, Alberta, Canada.
- Murphey, C. E., Langner, C. G., 1985. "Ultimate Pipe Strength under Bending, Collapse and Fatigue. In: Proceedings of the 4th International Conference on Offshore Mechanics and Arctic Engineering, Dallas, USA.
- Pasqualino, I., P., Neves, H., G., 2010. Collapse pressure of reeled rigid. In: Proc. of the 33th International Conference on Offshore Mechanics and Arctic Engineering, St John's, Canada.
- Pasqualino, I., Silvia, S. S., Estefen, S. F., 2004. The effect of the reeling laying method on the collapse pressure of steel pipes for deepwater. In: Proc. of the 23th International Conference on Offshore Mechanics and Arctic Engineering, San Francisco, California.
- Sriskandarajah, T., Rao, V., 2015. Predictive residual ovality for reel-laid pipelines in deepwater. In: Proc. of the 33th International Conference on Offshore Mechanics and Arctic Engineering, St John's, Canada.
- Ucak, A., Tsopelas, P., 2011. Constitutive model for cyclic response of structural steels with yield plateau. *J. Struct. Eng.* 137 (2), 195–206.
- Zhang, Z. L., Østby, E., Nyhus, B., Ødegård, J., Verley, R., 2004. Reeling-induced residual stress and its effect on the fracture behaviour of pipes with through thickness cracks. In: Proc. of the 4th International Conference on Pipeline Technology, Ostend, Belgium.